Check for updates

Systematic investigation of the adsorption potential of lignin- and cellulose-based nanomaterials towards pharmaceuticals†

Melissa B. Agustin, [iD] *[a] Kirsi S. Mikkonen, [iD] [ab] Marianna Kemell, [iD] [c] Panu Lahtinen[d] and Mari Lehtonen [iD] [a]

Pharmaceuticals are emerging water pollutants that pose a global threat to the sustainability and safety of aquatic resources. To mitigate their potential hazardous impacts, one of the keys is to address the removal of pharmaceutical residues from wastewaters. In this study, adsorption utilizing nanostructured wood-based adsorbents is viewed as a simple and versatile wastewater treatment method that can be adapted to remove pharmaceutical pollutants. To realize this potential, there is a need to understand the interaction of wood-based nanomaterials towards various types of pharmaceuticals. Thus, this study characterized and investigated the adsorption potential of the two common wood-based nanomaterials, the nanocelluloses and lignin nanoparticles (LNPs), towards various types of pharmaceuticals. The unmodified and cationized LNPs from hardwood and softwood lignin and nanocelluloses (TEMPO-oxidized cellulose nanofibrils (TCNF), cellulose and lignocellulose nanofibrils) were characterized for their morphology, zeta potential and surface charge density at different pHs. The adsorption capacity was determined from a multi-analyte adsorption system consisting of seven pharmaceuticals with different chemical characteristics (aromatic, non-aromatic, anionic, cationic, and neutral). Overall, the LNPs, with their polyaromatic structure, adsorbed a wider range of pharmaceuticals than the nanocelluloses. Among the nanocelluloses, the TCNF exhibited the highest adsorption capacity for cationic pharmaceuticals. Based on these findings, LNPs and TCNF are promising materials that can be combined to construct novel nanostructured adsorbents for pharmaceutical pollutants in water. The interaction of different pharmaceuticals with LNPs and nanocelluloses as revealed in this study can also be beneficial in other applications, such as drug encapsulation and release.

Environmental significance

Pharmaceutical pollution is a global environmental problem posing ecological and human health hazards. As one of the main routes of entry of pharmaceuticals into aquatic environments is *via* municipal wastewaters, their removal from wastewaters is important to mitigate their impacts. Adsorption using adsorbents that are highly specific towards pharmaceutical compounds, at the same time efficient and reusable, is a simple and versatile method to address pharmaceutical pollution. These novel adsorbents can be engineered from wood-base nanomaterials such as nanocelluloses and lignin nanoparticles, while simultaneously responding to a call for green and sustainable manufacturing processes. Understanding the interaction of these wood-based nanomaterials towards various types of pharmaceuticals is a foundation that will optimize the development of nanostructured wood-based adsorbents.

[a] Department of Food and Nutrition, Faculty of Agriculture and Forestry, University of Helsinki, P.O. Box 66, FI-00014, Finland

[b] Helsinki Institute of Sustainability Science, University of Helsinki, P.O. Box 65, FI-00014, Finland

[c] Department of Chemistry, Faculty of Science, University of Helsinki, P.O. Box 55, FI-00014, Finland

[d] VTT, Technical Research Centre of Finland, P.O. Box 1000, FIN-02044 VTT, Finland

Introduction

Pharmaceuticals, either synthetic or natural chemicals found in various types of medical and veterinary drugs, undeniably protect and cure millions from various types of diseases. Ironically, this same group of chemicals has been for the past decades one of the contaminants of emerging concern. They are not subjected to regular monitoring but they could enter the environment and pose or cause adverse ecological and human health effects.[1] Though these drugs typically pass rigorous tests for their safety at normal dose thresholds, their compiling residues in the environment have been linked to

2006 | *Environ. Sci.: Nano*, 2022, **9**, 2006–2019

This journal is © The Royal Society of Chemistry 2022

behavioral changes[2–4] and endocrine disruption[5–7] of some aquatic organisms. In addition, pharmaceutical residues, antibiotics in particular, have been associated with the emergence of antibiotic-resistant microorganisms.[8]

Pharmaceuticals have been detected in all types of water compartments including surface water, groundwater, tapwater, and even in drinking water in various parts of the world.[9,10] One of their main entry routes in to the aquatic environment is through effluent from municipal wastewater treatment plants.[10] This is because when medicines are consumed, approximately 70% of the active ingredient is excreted in the urine.[11] The excreted medicines combine with municipal wastewaters, which, even after passing through wastewater treatment procedures still contain residual pharmaceutical compounds. In line with this, the European Commission proposed the improvement in wastewater treatment technology as one of the strategic approaches to mitigate the negative impacts of pharmaceutical pollution.[12]

The development of efficient, cost-effective and scalable methods for removing pharmaceutical pollutants is a current global challenge. Several methods have been proposed including the use of membrane bioreactors, advanced oxidation processes, enzymes, and nanomaterials as adsorbents or photocatalysts.[13–15] Among these methods, adsorption offers the advantages of having a simple design and operation, consuming less energy, and not producing degradation byproducts that can potentially be more toxic than the target pollutants.[16] It is already one of the conventional wastewater treatment methods that is often used at the final stage or as a tertiary treatment to remove trace amount of organic pollutants from the effluent before disposal.[17] Powdered activated carbon is an efficient adsorbent, but its high cost, production method that has negative environmental impacts, and difficulty for regeneration, call for the development of new alternatives.[18]

Technological advancement has enabled the development and utilization of nanoscale materials for water treatment. Nanomaterials in various forms (*e.g.*, rods, fibrils, tubes, spheres) and with varying composition (organic, inorganic, or hybrid) were engineered to produce nanostructured adsorbents characterized with large surface area to volume ratio, and high affinity and selectivity towards the target compounds.[19] Recently, a growing interest on the use of bio-based nanomaterials has emerged due to their lower carbon footprints compared to traditional fossil-based resources. Wood-based nanomaterials, such as nanocelluloses and lignin nanoparticles (LNPs) are attractive candidates as they are highly abundant, renewable, and they do not compete with food production. Nanocelluloses, in the form of nanofibrils or nanocrystals, gained significant research interest in water treatment applications as summarized in various reviews.[20–23] However, most of the applications include the removal of heavy metals, inorganic anions such as phosphates and nitrates, dyes, and oil.[20,24] Although

reports on the adsorption potential of lignin either as chemically modified lignin or as lignin-derived activated carbon are numerous,[25,26] the application of LNPs in water treatment is relatively unexplored. Moreover, applications targeting the removal of pharmaceutical compounds are limited. Thus, basic understanding of pharmaceutical adsorption potential and relevant mechanisms of nanocelluloses and LNPs is needed. The knowledge on their affinities towards pharmaceuticals provide insights for the future engineering of nanostructured wood-based adsorbents. Hence, in this study, we investigated the adsorption potential of various types of nanocelluloses: neutral cellulose nanofibrils (CNF), lignin-containing cellulose nanofibrils (LCNF), and anionic TEMPO-oxidized cellulose nanofibrils (TCNF); and LNPs, the unmodified anionic form and the cationic form, both from hardwood and softwood lignin. Adsorption of multiple active pharmaceutical ingredients (APIs) having different chemical properties were investigated in a model solution with varying concentration. The selected pharmaceuticals were also either in the list of top 20 most sold or measured in highest concentrations in waste and surface waters in the Baltic Sea Region.[27]
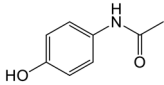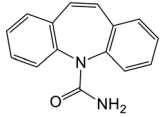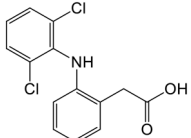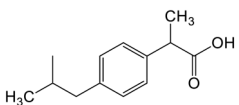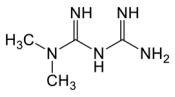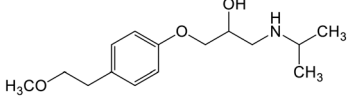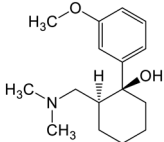
Experimental

Materials

The softwood Kraft Lignoboost lignin was provided by Stora Enso (Finland) while the hardwood birch BLN lignin was supplied by CH-Bioforce Oy (Finland). Detailed chemical characterization of the lignin samples has been previously published.[28] The TCNF and LCNF were both made of Nordic softwood Kraft pulp and were prepared following Skogberg *et al.* (2017)[29] and Lahtinen *et al.* (2014),[30] respectively, except that for the LCNF, the pulp was fibrillated seven times through a grinder to obtain fine fibrils. The softwood CNF was obtained from Research Institute of Sweden. The APIs (Table 1) were purchased from Sigma-Aldrich (Finland). Other chemicals such as the glycidyltrimethylammonium chloride (GTAC), and solvents, namely acetonitrile and methanol, used for chromatographic analysis were purchased from Sigma-Aldrich (Finland) and Fisher Scientific (Finland), respectively. The cationic poly(diallyldimethylammonium chloride) (PDADMAC) and anionic polyethylenesodiumsulfonate (PESNa) titrants were supplied by BTG Instruments (Finland).

Preparation of lignin nanoparticles

LNPs were prepared based on Farooq *et al.*, (2019).[31] Briefly, one gram of lignin was dissolved in 100 mL of 3 : 1 v/v acetone : water mixture and stirred at room temperature for 3 hours. The mixture was filtered (Whatman GF/F, pore size 0.7 μm) to remove undissolved materials, and the filtrate was poured in to 200 mL of deionized water that was being stirred rapidly. The acetone was removed by vacuum rotary evaporation at 40 °C.

Table 1 List of the studied pharmaceutical compounds

Active pharmaceutical ingredient	Abbreviation	Chemical structure	CAS number	Weighed form	Form in water	pK_a* (acid form)	Log K_{ow}*
Acetaminophen	ACE		103-90-2	Acetaminophen	Neutral	9.4	0.46
Carbamazepine	CBZ		298-46-4	Carbamazepine	Neutral	14	2.5
Diclofenac	DCF		15307-86-5	Diclofenac sodium salt	Anionic	4.2	4.5
Ibuprofen	IBU		15687-27-1	Ibuprofen	Anionic	4.9	4.0
Metformin	MTF		657-24-9	Metformin hydrochloride	Cationic	12	−2.6
Metoprolol	MTP		37350-58-6	Metroprolol tartrate	Cationic	9.6	1.9
Tramadol	TRA		27203-92-5	Tramadol hydrochloride	Cationic	9.4	3.0

pK_a and log K_{ow} values were obtained from a database available at **https://pubchem.ncbi.nlm.nih.gov/**.

Cationization of lignin and preparation of cationic lignin nanoparticles

Cationic lignin was prepared by reacting lignin with GTAC at 2∶1 mole ratio of GTAC to phenolic content of lignin.[32,33] One gram of lignin was mixed with 15 mL 0.2 M NaOH and stirred to completely dissolve the lignin. GTAC was added dropwise and the mixture was maintained at 70 °C for 1 h. The mixture was neutralized with 0.2 M sulfuric acid and then dialyzed using Spectra/Por (MWCO 1 kDa) against deionized water for four days, changing the water three times per day. The final mixture was centrifuged at 3400g for 10 min to separate any insoluble lignin and the supernatant was used for further work.

The synthesized soluble cationic lignin was used to cationize the surface of the isolated LNPs by electrostatic attraction according to Sipponen et al., (2017).[34] The LNPs were coated with cationic lignin by mixing the water soluble cationic lignin with LNP suspension in varying ratios (25–400 mg cationic lignin per gram LNP based on dry weight). The mixture was stirred for 5 min, transferred to a Spectra/Por 1 dialysis tube with MWCO 6–8 kDa, and dialyzed for three days against deionized water.

Characterization

The total amount of phenolic hydroxyls was determined spectrophotometrically by Folin–Ciocalteu method.[35,36] Briefly, 0.05 mL of solubilized lignin in alkaline solution (0.5 mg mL^{-1}) was diluted with 1.8 mL of MilliQ-water and mixed with 0.15 mL Folin–Ciocalteu reagent. The mixture was allowed to stand for 6 min before adding 0.5 mL sodium carbonate solution (20% w/w). The mixture was agitated in a water bath kept at 40 °C for 30 min before measuring the absorbance at 760 nm with an UV-vis spectrophotometer (UV-1800 Shimadzu). The amount of free phenolic groups was determined against vanillin standard curves.

The average hydrodynamic diameter (D_H) and ζ-potential at various conditions of the lignin-based samples were determined by dynamic light scattering using the Zetasizer Nano-ZS Zen 3600 (Malvern Instruments Ltd., Worcestershire, U.K.). Lignin nanoparticles suspension (0.5 mg mL^{-1}) was transferred into a folded capillary cell, equilibrated at 25 °C and illuminated with a laser (4 mW, 632.8 nm). The intensity of the back scattered light was measured by a detector positioned at 173°. For the ζ-potential measurement, an electric field of 40 V was applied and the electrophoretic

mobility data obtained from the measurement were converted to the ζ-potential using the Smoluchowski model. All data were processed using the built-in Zetasizer software version 7.13. To adjust the pH of the sample, either aqueous 0.1 M NaOH or 0.1 M HCl were added depending on the desired pH. Measurements were performed one hour after pH adjustment.

The morphology of the lignin- and cellulose-based nanomaterials was examined by a field emission scanning electron microscope (S-4800, Hitachi, Japan). A small portion of the freeze-dried samples was adhered on to a carbon tape and coated with 3–5 nm Au–Pd alloy. For the lignin-based nanoparticles, the diameter of at least 200 particles was measured using the SPM data visualization and analysis tool Gwyddion v2.55.

The charge density of the samples (soluble cationic lignin, LNPs, cationic LNPs (cLNPs), and nanocelluloses) was estimated by polyelectrolyte titration using a Mütek™ PCD-05 particle charge detector (BTG Instruments GmbH, Herrsching, Germany) in conjunction with an Omnis autotitrator (Metrohm Corp., Switzerland). A 10 mL suspension of the anionic samples was titrated directly with a 0.001 N PDADMAC while cationic samples were reacted with an excess of 0.001 N PESNa and back titrated with PDADMAC. The charge density was determined at different pH values (3, 5, 8.5), which were adjusted before the titration with 0.1 M NaOH or 0.1 M HCl.

Adsorption experiment

The initial screening for the adsorption potential of the nanomaterials was performed using aqueous solutions containing 20 mg L^{-1} of each pharmaceutical. A known mass of the freeze dried nanomaterials was mixed with the pharmaceutical solution to a fixed mass (g) to volume (mL) ratio of 1 : 1. The mixture was stirred for 1 h using a multiple stirrer plate at room temperature. The 1 hour duration was chosen based on the results of the preliminary time-series experiment (Fig. S1†), which showed no significant change in adsorption capacity after 1 h. After which, the mixture was centrifuged at 3400g for 10 min and the supernatant was further filtered using a syringe filter (0.45 μm, Acrodisc WWPTFE membrane). At least three independent analyses, with random replications, were performed. For each independent analysis, a blank sample containing only the pharmaceuticals was prepared and analyzed the same way as the treated samples. The initial concentration used when calculating the adsorption capacity was then set based on the results of the blank analysis. This was done in order to eliminate the effect of potential adsorption on the surfaces of the materials during the experiment. For the effect of varying the pH, the same procedure was followed, except that the pH of the pharmaceutical solution was first adjusted to 3 and 8.5 using 0.1 M HCl and 0.1 M NaOH, respectively, before mixing with the adsorbent. The effect of varying the initial pharmaceutical concentration was performed following the

same procedure and the concentrations used were 5, 10, 20, 40, 80, and 100 mg L^{-1}.

Quantitation of active pharmaceutical ingredients by UHPLC-PDA

Adsorption efficiencies of investigated materials was determined by quantifying APIs by ultra-high performance liquid chromatography (UHPLC) combined with UV/vis detection (PDA). For the analysis, 0.8 mL of the filtered sample was mixed with 0.2 mL of methanol. Five microliters was injected in to an Acquity HSS T3 C18 column (2.1 × 100 mm, 1.8 μm) connected to Waters Acquity UPLC system (Waters, Milford, MA, USA) equipped with a photodiode array detector. Separation was achieved by gradient elution from 80% of 0.1% formic acid to 99% acetonitrile in 6 min at a flow rate of 0.4 mL min^{-1}. Quantitation of seven different APIs ACE (244 nm), CBZ (276 nm), DCF (276 nm), IBU (284 nm), MTF (244 nm), MPL (223 nm) and TRA (272 nm) was based on external standard method at concentration ranges of 0.1–40 mg L^{-1}.
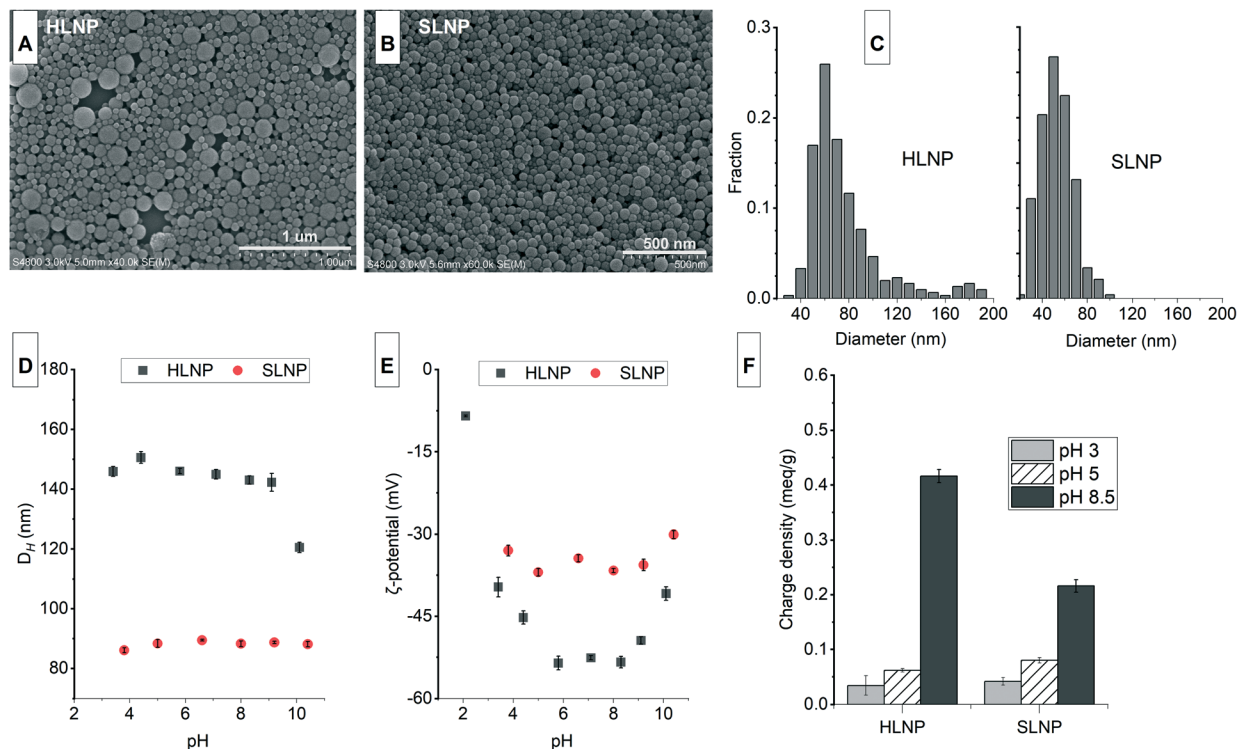
Results and discussion

The studied nanomaterials were characterized for their morphology, ζ-potential, DH and surface charge density at various pHs. The properties at differing pH gives an indication of their stability and function at various adsorption conditions.

The characteristics of unmodified lignin nanoparticles

The isolation of LNPs by acetone nanoprecipitation is a rapid, simple and effective method of preparing spherical and stable LNPs.[28] As shown in Fig. 1A and B, the morphology of the isolated LNPs remained spherical even after freeze drying. About 85% of the hardwood LNPs (HLNPs) have <100 nm diameter and the size distribution peaked at 60 nm. The presence of larger particles (diameter > 100 nm) is evident in the HLNP and this is also reflected in the wide frequency size distribution plots (Fig. 1C). The softwood LNPs (SLNPs) exhibited a narrower size distribution than that of the HLNPs, and the particle diameter peaked at 50 nm. The average D_{H} (150 nm for HLNPs and 90 nm for SLNPs) as expected were larger than the diameter obtained from the FESEM. The D_{H} from DLS is the apparent diameter of the solvated particle that is approximated as a hard sphere, while the FESEM diameter reflects the 'dry state' or 'internal core' of the particle.[37] The average D_{H} for both particles was stable at pH 3 to 9. However, at pH 10, the D_{H} of HLNPs decreased attributed to the partial dissolution of the particles evident from the darkening of the suspension. The ζ-potential of the isolated LNPs showed a typical anionic character of lignin depicted from highly negative ζ-potential values (Fig. 1E). The HLNPs have a slightly more negative ζ-potential attributed to it having a higher number of carboxylic groups (0.62 over 0.35 mmol g^{-1}) based on the previous P-NMR analysis of the same materials.[28] Typical with lignin, the ζ-potential was less negative at pH

This journal is © The Royal Society of Chemistry 2022

Environ. Sci.: Nano, 2022, **9**, 2006–2019 | **2009**

Fig. 1 The morphology (A and B), frequency size distribution plots (C), changes in average hydrodynamic diameter (D_H, D), ζ-potential (E), and charge density (F) as affected by pH variation of the isolated hardwood (HLNP) and softwood (SLNP) lignin nanoparticles. Error bars represent ± standard deviation of at least three replicates.

below 5 due to protonation of the carboxyl groups. The ζ-potential values were at its lowest between pH 5 and 8, and started to increase from pH 9. This unusual increase in ζ-potential of LNPs at highly alkaline conditions was also observed by others.[28,38] One of the possible reasons could be the dissolution of LNPs at pH above 9, indicated by the formation of dark color in the suspension. This dissolution could alter the surface of the LNPs and the surrounding medium, which could have an effect on the electric double layer of the particles, and on their mobility, ultimately affecting the ζ-potential. Although, the ζ-potential values were highly negative, the surface charge density, which is dependent on the number of charged functional groups bound to the particles,[39] were quite low (Fig. 1F). At pH 5, the anionic surface charge density was <0.1 meq g^{-1} and further decreased at pH 3 because of the protonation of the carboxyl groups. At pH 8.5, deprotonation of carboxyl groups resulted in an increase in charge density.
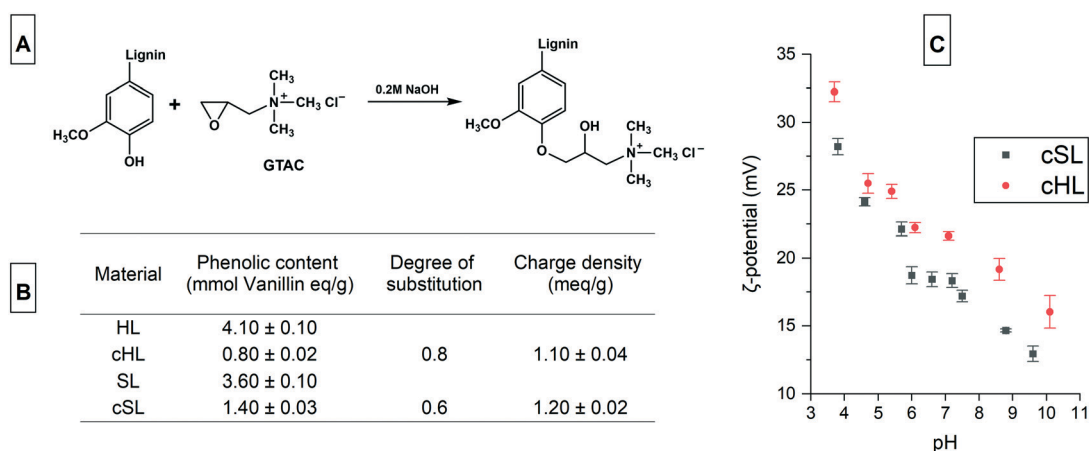
Fig. 2 The reaction scheme showing the cationization of hardwood (HL) and softwood (SL) lignin with glycidyltrimethylammonium chloride, GTAC (A), the phenolic content, degree of substitution, and charge density of the water soluble cationic hardwood (cHL) and softwood (cSL) lignin (B) and the variation in ζ-potential of the cationic lignin as affected by pH (C).

| Material	Phenolic content (mmol Vanillin eq/g)	Degree of substitution	Charge density (meq/g)
HL	4.10 ± 0.10		
cHL	0.80 ± 0.02	0.8	1.10 ± 0.04
SL	3.60 ± 0.10		
cSL	1.40 ± 0.03	0.6	1.20 ± 0.02

The characteristics of cationic lignin nanoparticles

Soluble cationic lignin was first prepared from lignin, which is typically water insoluble and anionic. Cationization by the introduction of quaternary ammonium ions makes lignin positively charged and increases their solubility in water. The reaction of lignin with GTAC (Fig. 2A), an epoxide carrying a quaternary ammonium ion, proved to be effective in preparing cationic lignin.[32] The method is a rapid, one-pot, one-step synthesis that does not require hazardous organic solvent for the dissolution of the lignin. The reaction is performed in aqueous alkaline condition that promotes the dissolution of lignin, at the same time, activates the phenolic hydroxyls by deprotonation.[33]

The cationization of HL and SL yielded cationic lignin products which had a water solubility of more than 90%, a similar degree of solubility to that obtained from the cationization of a softwood Kraft lignin, previously reported.[32] Since the chemical selectivity of the nucleophilic attack on the epoxide group of GTAC favors the phenolate anion, which is more nucleophilic than aliphatic hydroxyls, the degree of substitution (DS) is calculated from the amount

of phenolic hydroxyls before and after cationization.[33] As shown in the inset table in Fig. 2, the DS of the cHL and cSL were 0.8 and 0.6, respectively. These values are comparable to the 0.74 DS value obtained from the 20 h reaction at 60 °C of a hardwood organosolv lignin with GTAC, also at a similar mole ratio of 2:1 GTAC to phenolic content.[33] A similar softwood Kraft Lignoboost lignin also exhibited 65% conversion (DS 0.65) of the phenolic content following the same cationization procedure.[34] The charge density of the cationic lignin also reached 1.2 meq g^{-1} and the ζ-potential showed a decreasing trend with increasing pH because of carboxyl group deprotonation (Fig. 2C).

The synthesized soluble cationic lignin was used to coat the surface of the anionic LNPs at different dry mass ratios of cationic lignin to LNP (cLignin:LNP). The soluble cationic lignin adhered to the anionic surface of the LNPs because of electrostatic attraction. At ratios below 100 mg g^{-1}, the LNPs agglomerated because of the neutralization of the negative charge as shown in the increase in ζ-potential from negative to almost neutral (Fig. 3A and B). As the amount of cationic lignin was increased, the negative charge was completely neutralized and the cationic lignin dominated the surface
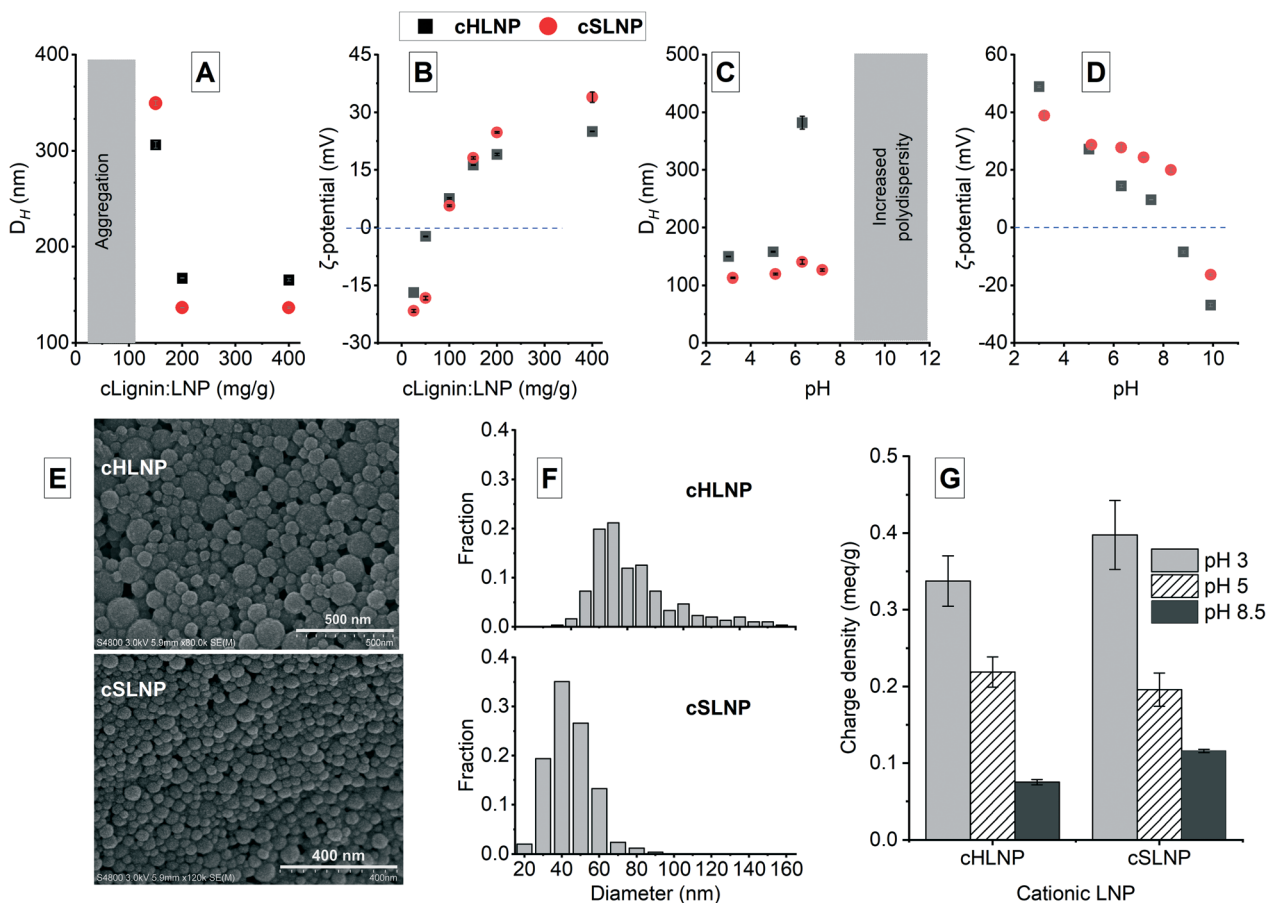
Fig. 3 The formation of stable cationic hardwood (cHLNP) and softwood (cSLNP) lignin nanoparticles (LNPs) monitored by the changes in hydrodynamic diameter (D_H) and ζ-potential with increasing dry mass ratio of the soluble cationic lignin (cLignin) to LNPs (A and B); the variation in D_H (C) and ζ-potential (D) with pH, the morphology (E), frequency size distribution (F), charge density (G) and cationic LNPs with 400:1 mg g^{-1} cLignin:LNP ratio.

This journal is © The Royal Society of Chemistry 2022

Environ. Sci.: Nano, 2022, **9**, 2006–2019 | **2011**

charge of the coated LNPs (Fig. 3A and B). The cLNPs prepared at 400 mg g^{-1} had the highest positive charge, and was further characterized and chosen for the adsorption studies. The cLNPs were not stable at pH above 8.5 indicated by an increase in polydispersity possibly due to partial dissolution or agglomeration of the particles (Fig. 3C). This agglomeration could be brought by the deprotonation of the carboxyl groups, which form electrostatic attraction with the cationic ternary ammonium groups on the other particle. As a result of this attraction, charge neutralization occurred and the ζ-potential became less positive (Fig. 3D). The LNPs remained spherical (Fig. 3E) even after coating with cationic lignin and the frequency size distribution remained essentially the same, with the cationic HLNPs (cHLNPs) having a wider distribution than the cationic SLNPs (cSLNPs) (Fig. 1F). The surface charge density of the cLNPs also varied with the pH and followed a trend similar to that of the ζ-potential (Fig. 3G). At pH 3, the cLNPs were highly positive while at pH 8 the cationic surface charge density decreased because of the deprotonation of the carboxyl groups.

The cellulose-based nanomaterials

The cellulose-based nanomaterials include the neutral CNF, the LCNF with 3% lignin, and the negatively charged TCNF. The LCNF is an emerging family of cellulose-based nanomaterials and has displayed different behaviors than the pure CNF because of the presence of lignin.[40] Unlike LNPs that are spherical, these cellulosic nanomaterials consist of entangled, long nanofibrils of varying widths (Fig. 4). The TCNF had widths of less than 10 nm and was the smallest, while the LCNF (~15–20 nm) was slightly smaller than the CNF (~25–30 nm). The lignin in the LCNF appeared as precipitated, irregularly shaped particles on the surface of the nanofibrils. The surface charge density of TCNF was highly negative at 1.3 meq g^{-1}, as expected because of the C6-carboxylation during TEMPO-oxidation.[41] The CNF and LCNF, both also had a net negative charge, having a charge density of 0.03 and 0.07 meq g^{-1}, respectively. The higher charge density of LCNF compared to CNF was attributed to the presence of lignin and higher hemicellulose content compared to the fully bleached softwood pulp used for CNF production.

Adsorption capacity

Adsorption is a surface phenomenon that involves the interaction of the target adsorbate, *i.e.* the pollutants in the case of wastewater treatment, and that of the surface of a solid adsorbent.[42] Various types of interactions such as electrostatic, H-bonding, hydrophobic, or π–π stacking occur between the adsorbent surface and the target adsorbate.[43] These interactions lead to the accumulation of the adsorbate on the surface of the adsorbent. The amount of adsorbed materials at a given time, known as the adsorption capacity, q, in mg g^{-1} is calculated from the equation:

$$q = \frac{(C_O - C_f)V}{m}$$

where C_O and C_f are the initial and final concentration (mg L^{-1}), respectively, V is the volume (L) of the solution, and m is the dry mass in grams of the adsorbent.

The q values of each nanomaterial for different types of pharmaceuticals are presented in Fig. 5. The q values varied and could be linked to the varying interaction of the nanomaterials with the pharmaceuticals having different chemical characteristics. Results showed that electrostatic attraction proved to be a strong driving force for the adsorption of charged pharmaceuticals by charged nanomaterials. The cHLNPs and cSLNPs gave the highest average q for DCF (11.8 mg g^{-1}) and IBU (6.8 mg g^{-1}), which have both anionic carboxyl groups. The higher adsorption for DCF (pK_a 4.1) over IBU (pK_a 4.9) could be due to a higher degree of ionization of DCF at pH 5. Meanwhile, the highly negative TCNF gave the highest q for the three cationic pharmaceuticals, MTF (7.6 mg g^{-1}), MPL (7.3 mg g^{-1}) and TRA (6.6 mg g^{-1}), and did not show affinity towards neutral or anionic pharmaceuticals ($q < 0.1$ mg g^{-1}). Similarly, the unmodified LNPs, which are naturally anionic, but with lower surface charge than TCNF, were able to adsorb MTF (1.3 mg g^{-1}), MPL (6.3 mg g^{-1}) and TRA (4.7 mg g^{-1}). The CNF and LCNF showed very weak adsorption potential. These two nanomaterials have very low charge density, and possibly were not able to establish electrostatic attraction. The potential mode of removal *via* H-bonding with the hydroxyl groups of the glucose units in cellulose seemed not sufficient
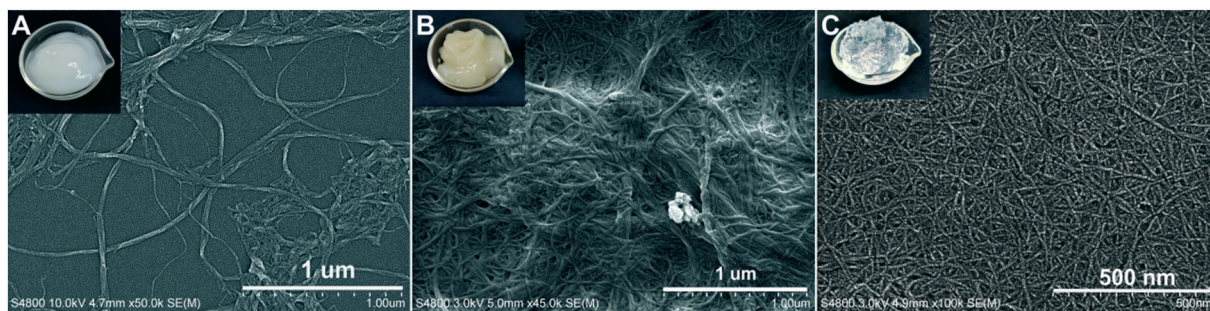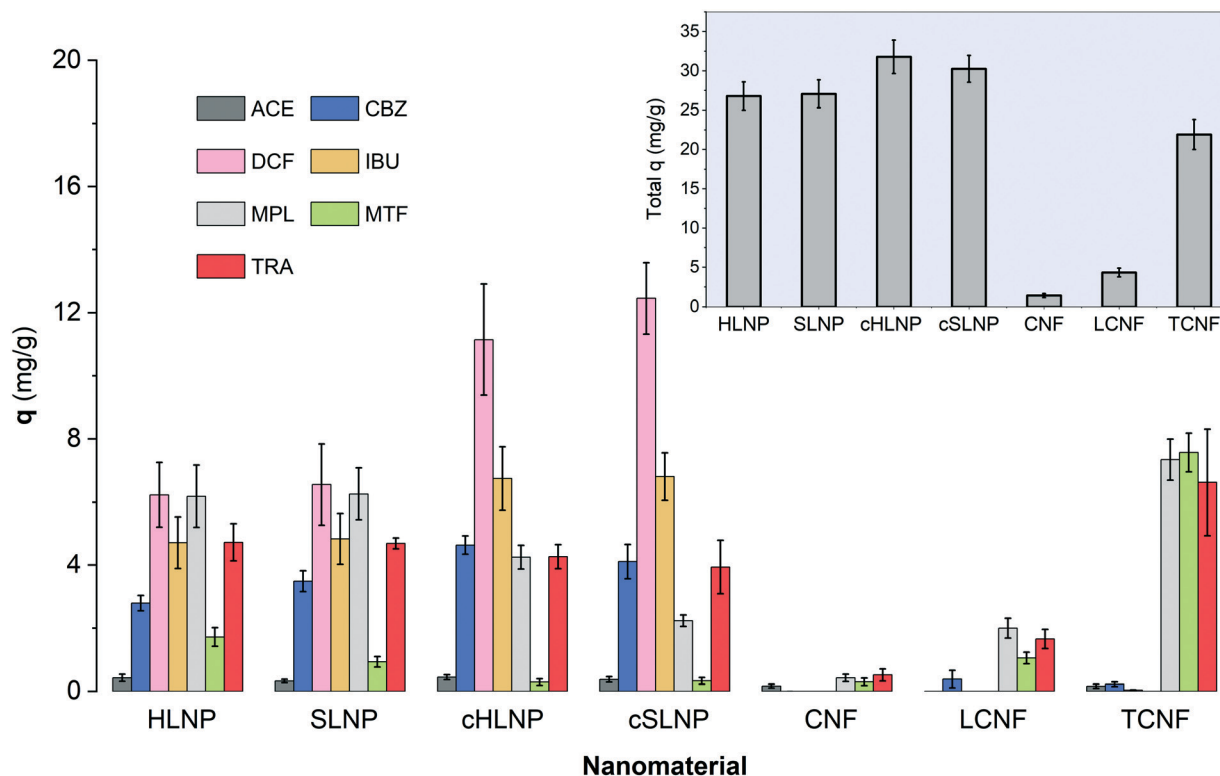

Fig. 4 FESEM images of cellulose nanofibrils (A), lignocellulose nanofibrils (B) and tempo-oxidized cellulose nanofibrils (C) and photos of their corresponding suspension as insets.

2012 | *Environ. Sci.: Nano*, 2022, **9**, 2006–2019

This journal is © The Royal Society of Chemistry 2022

Fig. 5 The amount of adsorbed pharmaceutical in mg per gram of nanomaterial, the adsorption capacity, q, of lignin- and cellulose-based nanomaterials for different types of pharmaceuticals. Inset is the total q of each nanomaterial. Adsorption conditions: room temperature, 1 h, 20 μg ml^{-1} initial concentration, 1 mg mL^{-1} mass to volume ratio of adsorbent to pharmaceutical solution, pH $\approx$ 5. Error bars represent $\pm$ standard deviation of at least five measurements.

enough to remove the pharmaceuticals having amine, carboxyl and hydroxyl groups. It is interesting to note that the presence of lignin in LCNF, even for only 3%, imparted a difference in adsorption potential in comparison with CNF. The small amount of lignin in LCNF seemed to enhance the adsorption of cationic pharmaceuticals. The CNF had a $q <$ 0.5 mg g^{-1} for the cationic MPL, MTF, and TRA while a q of 2.0, 1.1 and 1.7 mg g^{-1}, respectively, was observed for the LCNF. This improvement could be due to the anionic character of the residual lignin in the LCNF.

Apart from electrostatic attractions, π–π interactions seemed to contribute significantly towards the removal of aromatic pharmaceuticals by the polyaromatic LNPs. This is evident from the following observations: (1) the cationic aromatic MPL and TRA were moderately removed by cHLNPs (4.2 mg g^{-1}) and cSLNPs (3.1 mg g^{-1}) despite similarities in their charge, while the MTF, that is cationic but non-aromatic was poorly removed ($q <$ 0.3 mg g^{-1}); (2) the negatively charged IBU and DCF were also moderately removed by unmodified, anionic HLNPs and SLNPs (average q of 5.6 mg g^{-1}), while the TCNF that was highly negative but without aromatic groups, clearly could not remove IBU and DCF ($q <$ 0.1 mg g^{-1}); and (3) the neutral CBZ was moderately removed by lignin-based nanomaterials (average q of 3.8 mg g^{-1}) regardless of the charge of the LNPs, but was poorly removed by CNF or TCNF ($q <$ 0.2 mg g^{-1}).

Overall, the total q, calculated by taking the sum of the q values of each pharmaceuticals per nanomaterial, did not show huge differences between the unmodified and cationic LNPs. Furthermore, the source of LNP, whether from hardwood or softwood, did not show significant difference on q. Among the nanocelluloses, the TCNF had the highest total q, mainly brought by its capacity to remove cationic pharmaceuticals.

Effect of pH on adsorption. The pH of a solution affects the speciation of pharmaceuticals and nanomaterials, which may either increase or decrease the adsorption capacity. The speciation of pharmaceuticals as a function of pH was calculated using the Henderson–Hasselbalch equation (Fig. S2†). Based on the calculations, the studied pharmaceuticals can be divided into three groups at pH 7: neutral (ACE, CBZ); anionic (IBU, DCF); and cationic (MPL, MTF, TRA). Similarly, the charge density of the studied nanomaterials, as discussed in the previous sections, varied with the pH. The q values of the selected nanomaterials for each pharmaceuticals at different pH values are shown in Fig. 6. A pH higher than 8.5 was not tested because of the potential dissolution of lignin at this conditions as observed in section 3.2. The adsorption of LCNF and CNF as affected by pH was not included because their adsorption potential were much inferior than the other nanomaterials as observed in the initial screening.

The adsorption of ACE towards the selected nanomaterials at various pH did not show a clear trend and was consistently
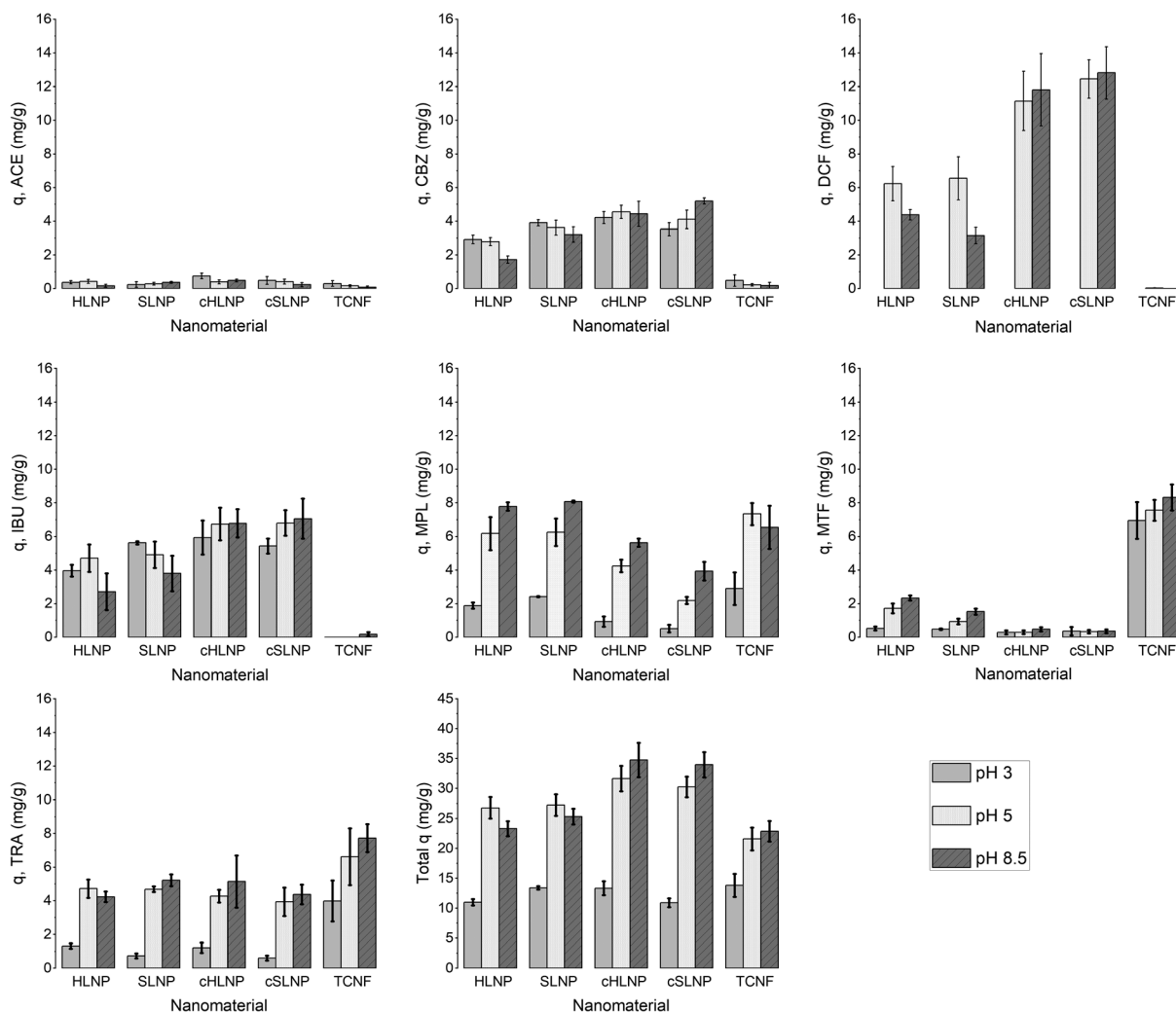
This journal is © The Royal Society of Chemistry 2022

Environ. Sci.: Nano, 2022, **9**, 2006–2019 | **2013**

Fig. 6 The adsorption capacity, q, of the different nanomaterials as affected by pH. Adsorption conditions: room temperature, 1 h, 20 μg mL^{-1} initial pharmaceutical concentration, 1 mg mL^{-1} mass to volume ratio of adsorbent to pharmaceutical solution. Error bars represent ± standard deviation of at least five measurements.

the lowest (average q of 0.3) among the pharmaceuticals tested. With a pKa of 9.4, corresponding to the dissociation of the phenolic hydroxyl, ACE remained in its neutral form at pH 3 and 5, with a small portion starting to dissociate at pH 8.5 (Fig. S1†). Because of being neutral, ACE was hardly removed from the water despite the changes in the charge densities of the studied adsorbents. The possible adsorption *via* H-bonding or π–π interactions did not cause significant removal of ACE. To understand if the poor adsorption was due to competition of ACE with other highly aromatic and charged pharmaceuticals, the adsorption potential was studied in a solution with only ACE present. Interestingly, the q values remained low ($q < 0.3$) indicating that the adsorption was not inhibited by competition. Apart from being neutral, the small size of ACE, in combination with its low log K_{ow} (0.46), are possible reasons for its low adsorption.

Similarly as ACE, CBZ (pK_a = 13.9) existed in its neutral, undissociated form at the studied pH range. However, since CBZ is more non-polar (log K_{ow} = 2.5) and has more aromatic

characteristics than ACE, CBZ was adsorbed more efficiently by the lignin-based nanomaterials. Possible interactions could be π–π aromatic rings stacking, H-bonding or hydrophobic interactions. The adsorption of CBZ onto charged TCNF, remained very low and did not show improvement at different pH.

The acidic pharmaceuticals, DCF (pK_a = 4.1) and IBU (pK_a = 4.9), were mostly neutral at pH 3, having only a fraction of less than 0.1 existing in the deprotonated form. At pH 5, both protonated and deprotonated carboxyl groups exist, while at pH 8.5, the anionic carboxylate form dominates. These different speciations affected the adsorption of DCF and IBU at different pH. At pH 3, the protonated form of DCF was insoluble in water and was therefore removed in the filtration prior to UHPLC analysis. The absence of DCF was apparent in chromatograms. Thus, the adsorption capacity for DCF was not assessed at pH 3. Comparing the adsorption at pH 5 and 8.5, cHLNPs and cSLNPs had almost two times higher q than the

unmodified, anionic LNP counterparts. Even though the surface charge density of cHLNPs and cSLNPs was much less positive at pH 8.5 than at pH 5, the q-values for DCF were the same at both conditions. This observation confirms that the adsorption of DCF was not only driven by electrostatic attraction but also by π–π aromatic interaction. For unmodified HLNPs and SLNPs the adsorption capacity decreased with an increasing pH. This behavior is most likely due to electrostatic repulsion because at high pH, both the DCF and the LNPs were highly negative.

The adsorption of IBU by HLNPs and SLNPs were generally higher at acidic conditions than at pH 8. At acidic pH, the HLNPs and SLNPs had much lower negative surface charge density and the IBU species were mostly neutral. Thus, electrostatic attraction was weak and the adsorption was most likely driven by the π–π interaction in the aromatic ring, by H-bonding or by hydrophobic interactions. At pH 8.5, both IBU and LNPs were highly negative, resulting to a decreased adsorption due to increased repulsion. For the cLNPs, the increase in the cationic charge at pH 3 did not seem to favor the removal of IBU because the dominant species of the IBU was the neutral form. At pH 5 and 8.5,

where IBU is mostly ionized, electrostatic attraction resulted in an increase in q for the cLNPs.

The basic pharmaceuticals, MPL, MTF and TRA, exist mostly as cations in the studied pH range. The adsorption capacity was therefore mostly defined by the speciation of the adsorbent with changing pH. As expected, an increase in the anionic character of the adsorbent increased its adsorption capacity for these cationic pharmaceuticals. Carboxyl groups of studied nanomaterials become deprotonated at elevated pH making them more accessible for electrostatic interaction with the positively charged amino groups in MPL, MTF and TRA. The anionic TCNF, which had the highest surface charge density, had the greatest adsorption capacity for these cationic pharmaceuticals. Additionally, the absence of aromatic and hydrophobic groups in MTF resulted in very weak attraction with the cLNPs.

Overall, the adsorption capacities of the studied materials were low at pH 3 where the nanomaterials exist primarily in a neutral state. The increase in anionic character due to dissociation of carboxyl groups, improved adsorption capacity, especially for cationic pharmaceuticals. LNPs, whether in its unmodified anionic form or in cationized form, adsorbed a

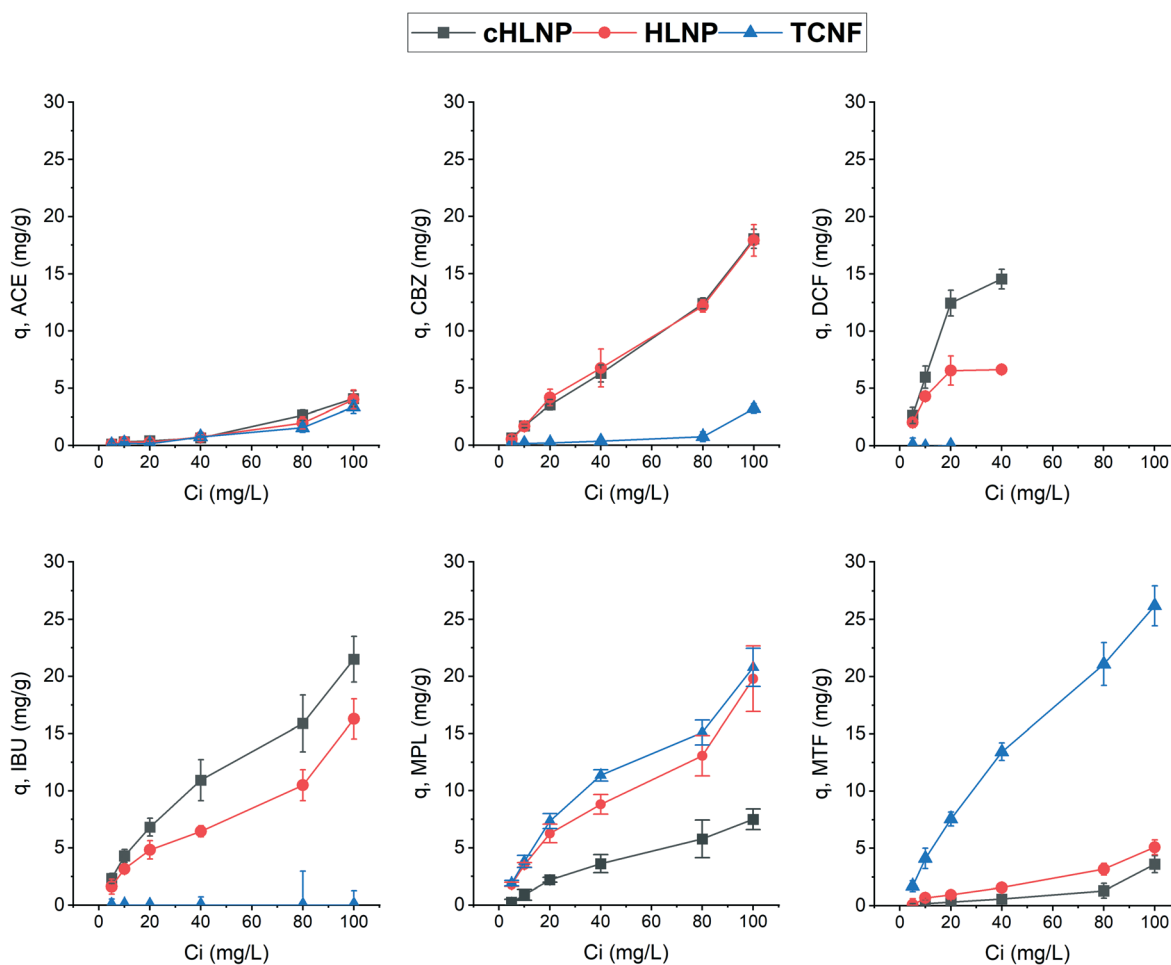**Fig. 7** The change in adsorption capacity, q, as affected by the initial concentration, Ci, of pharmaceuticals. Adsorption conditions: room temperature, 1 h, 1 mg mL^{-1} ratio of adsorbent mass to volume of solution, pH ≈ 5. Error bars represent ± standard deviation of at least five measurements.

This journal is © The Royal Society of Chemistry 2022

Environ. Sci.: Nano, 2022, **9**, 2006–2019 | **2015**

broader range of pharmaceuticals compared to TCNF. The adsorption capacity did not appreciably vary with the source of lignin even at different pH.

Effect of pharmaceutical concentration on the adsorption. The initial concentration of the adsorbate affects the adsorption capacity. When the initial concentration is high, the chance of collision between the adsorbate and adsorbent increased, enhancing adsorption. At the same time, competition of available adsorption sites increases resulting in less available places. As shown in Fig. 7, the adsorption capacities of cHLNP, HLNP, and TCNF increased with increasing initial concentration of the pharmaceuticals. Because the adsorption experiment was performed simultaneously for a mixture of six different pharmaceuticals, the curves were not fitted with adsorption isotherm models as mostly done in single-analyte adsorption system. The shape of the curves, however, could provide information about adsorbate–adsorbent interactions based on the IUPAC recommendations of classifications of adsorption isotherms.[44] Most of the curves display a type II adsorption isotherm characterized by a sigmoidal shape with one inflection point indicative of stronger adsorbent–adsorbate interaction than adsorbate–adsorbate interaction.[45] This type II

isotherm curve was observed in the adsorption of aromatic pharmaceuticals CBZ, IBU, and MPL towards LNPs and that of cationic MPL or MTF with TCNF. These results further confirm that the adsorption of aromatic pharmaceuticals is favored by their strong interaction towards lignin-based nanomaterials most likely *via* π–π aromatic ring interaction. Similarly, the removal of cationic pharmaceuticals by TCNF is driven by strong electrostatic attraction. Another type of shape observed was the type III isotherm adsorption characterized by an upward concave. This is seen in all the curves for ACE, that of the TCNF with CBZ, and between LNPs and MTF. The type III isotherm curve occurs when the attractive forces between the adsorbate and adsorbent are weaker than that between the adsorbate molecules.[45] The observed type III curves clearly agree with our findings for the low *q*-values of all adsorbents towards ACE, of lignin based-nanomaterials towards the non-aromatic, cationic MTF, and of TCNF towards aromatic neutral or anionic pharmaceuticals. The results for DCF at 80 and 100 mg L^{-1} was not shown due to poor dissolution at higher concentration at pH 5. Nevertheless, the affinity of DCF with cHLNP was consistent even at low concentration.

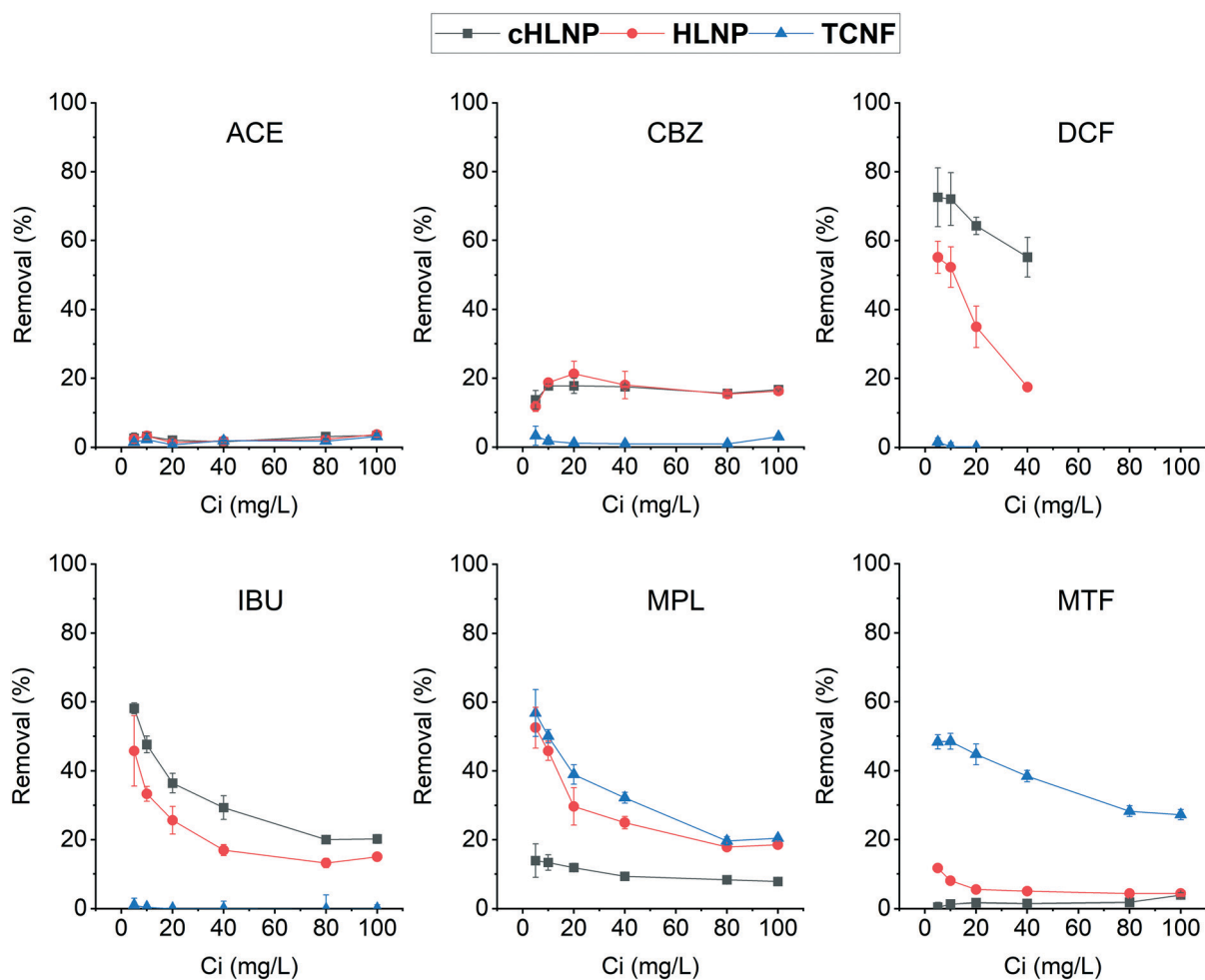**Fig. 8** The percentage removal as affected by the initial concentration, Ci, of pharmaceuticals. Adsorption conditions: room temperature, 1 h, 1 mg mL^{-1} ratio of adsorbent mass to volume of solution, pH ≈ 5. Error bars represent ± standard deviation of at least five measurements.

2016 | *Environ. Sci.: Nano*, 2022, **9**, 2006–2019

This journal is © The Royal Society of Chemistry 2022

To further assess the adsorption potential of the studied nanomaterials, the removal efficiency, expressed as percentage, at varying initial concentration was calculated and is presented in Fig. 8. As expected, with increasing concentration, the removal efficiency decreased, because the adsorbent eventually reached a saturation point and the amount adsorbed remains the same. Overall, the LNPs had higher removal efficiency for aromatic CBZ, DCF, and IBU than the TCNF. At a concentration below 10 mg L^{-1}, the cHLNP removed 70% of the DCF and 50% of the IBU. Both the cHLNP and HLNP showed an average of 20% removal for CBZ. For the aromatic cationic MPL, both the TCNF and HLNP performed a similar level of removal of 60% at 5 mg L^{-1}. For the aliphatic MTF, only the TCNF showed significant removal (50%), consistent with the observation that the lack of aromatic groups in MTF, coupled with being highly polar, rendered it difficult to interact with the LNPs. All the nanomaterials did not show significant removal for ACE and only removed an average of 3%.

Comparing the current findings with that of powdered activated carbon, which was able to achieve 95% removal for different pharmaceuticals including CBZ, DCF and MPL in a pilot scale set-up,[46] the studied nanomaterials seemed to be less efficient. However, it should be noted that removal efficiency depends on various factors and can greatly vary with the adsorption conditions. In particular, the range of concentrations of pharmaceuticals used in this study was at least order of magnitude higher than what is typically found in wastewaters. Considering a trend of decreasing removal with increasing concentration, a higher removal efficiency than what was observed could be expected if concentrations much lower than 5 mg L^{-1} are present.

Conclusions

The potential environmental and health hazards posed by pharmaceutical pollutants call for mitigation measures, one of which is improvement in wastewater treatment technologies. In this study, adsorption utilizing wood-based nanomaterials as adsorbents was considered as a simple water treatment method to address pharmaceutical pollution. Various types of nanocelluloses (CNF, LCNF, and TCNF) and unmodified and cationized LNPs from hardwood and softwood were screened for their adsorption potential. The selected pharmaceuticals for the study encompassed a broad range of chemical characteristics typical of what can be found in real wastewaters.

Thus, the interaction established by the nanomaterials to the selected pharmaceuticals in the model system could be extended to real scenarios. Similarly, the pH range used in the adsorption study covered the normal pH of wastewaters, which guaranteed the stability of the nanomaterials and their adsorption potential at different pH when in real conditions. Even though the range of pharmaceutical concentration was higher than those in wastewater, the findings enabled the identification of nanomaterials capable of removing pharmaceuticals from water and the types of interactions that drove the removal.

Overall, based on the results of this study, electrostatic attraction is a strong driving force that enabled the removal of either negatively or positively charged pharmaceuticals using oppositely charged nanocelluloses or LNPs. The LNPs could adsorb a broader range of pharmaceuticals than the nanocelluloses due to their additional capacity to interact via π–π aromatic ring stacking. The source of lignin, either softwood or hardwood, did not affect the adsorption behavior of the LNPs. The surrounding pH modifies the speciation of both nanomaterials and pharmaceuticals and could affect adsorption capacity. Among the studied nanomaterials, the TCNF and the unmodified and cationic LNPs, can be explored for engineering nanostructured adsorbents towards pharmaceuticals. A combination of these nanomaterials, for example by anchoring LNPs into the TCNF network, may provide a synergistic effect on adsorption behavior enabling more efficient removal of a wide range of different pharmaceuticals. Anchoring LNPs to a solid support would also ease their recovery from water after adsorption. For future studies, chemical characterization of the adsorbent after adsorption would be beneficial to establish the chemical interaction between pharmaceuticals and the adsorbent. Similarly, the adsorption kinetics of the adsorbent for each pharmaceutical would be worth exploring. Finally, regeneration and reusability studies, which were not included in this study, should be conducted for engineering sustainable and cost-effective future wood-based adsorbents.

Author contributions

Conceptualization, MBA, KSM, ML; funding acquisition, MBA; investigation, MBA; methodology, MBA, ML; resources, PL, MK; supervision, KSM, ML; visualization: MBA; writing – original draft, MBA; writing – review and editing, MBA, ML, KSM, PL, MK.

Conflicts of interest

There are no conflicts to declare.

Acknowledgements

References

1 V. Dulio, B. van Bavel, E. Brorström-Lundén, J. Harmsen, J. Hollender, M. Schlabach, J. Slobodnik, K. Thomas and J. Koschorreck, Emerging pollutants in the EU: 10 years of NORMAN in support of environmental policies and regulations, *Environ. Sci. Eur.*, 2018, **30**, 1–13.

This journal is © The Royal Society of Chemistry 2022

Environ. Sci.: Nano, 2022, **9**, 2006–2019 | **2017**

2 D. B. D. Simmons, E. S. McCallum, S. Balshine, B. Chandramouli, J. Cosgrove and J. P. Sherry, Reduced anxiety is associated with the accumulation of six serotonin reuptake inhibitors in wastewater treatment effluent exposed goldfish Carassius auratus, *Sci. Rep.*, 2017, **7**, 1–11.

3 T. Brodin, S. Piovano, J. Fick, J. Klaminder, M. Heynen, M. Heynen and M. Jonsson, Ecological effects of pharmaceuticals in aquatic systems – impacts through behavioural alterations, *Philos. Trans. R. Soc., B*, 2014, **369**, 20130580.

4 R. D. MacLaren, K. Wisniewski and C. MacLaren, Environmental concentrations of metformin exposure affect aggressive behavior in the siamese fighting fish, betta splendens, *PLoS One*, 2018, **13**, 6–8.

5 K. Kwak, K. Ji, Y. Kho, P. Kim, J. Lee, J. Ryu and K. Choi, Chronic toxicity and endocrine disruption of naproxen in freshwater waterfleas and fish, and steroidogenic alteration using H295R cell assay, *Chemosphere*, 2018, **204**, 156–162.

6 P. Kim, Y. Park, K. Ji, J. Seo, S. Lee, K. Choi, Y. Kho, J. Park and K. Choi, Effect of chronic exposure to acetaminophen and lincomycin on Japanese medaka (Oryzias latipes) and freshwater cladocerans Daphnia magna and Moina macrocopa, and potential mechanisms of endocrine disruption, *Chemosphere*, 2012, **89**, 10–18.

7 I. C. Guiloski, J. L. C. Ribas, L. D. S. Piancini, A. C. Dagostim, S. M. Cirio, L. F. Fávaro, S. L. Boschen, M. M. Cestari, C. da Cunha and H. C. Silva de Assis, Paracetamol causes endocrine disruption and hepatotoxicity in male fish Rhamdia quelen after subchronic exposure, *Environ. Toxicol. Pharmacol.*, 2017, **53**, 111–120.

8 G. K. Selvaraj, Z. Tian, H. Zhang, M. Jayaraman, M. Yang and Y. Zhang, Culture-based study on the development of antibiotic resistance in a biological wastewater system treating stepwise increasing doses of streptomycin, *AMB Express*, 2018, **8**(12), 1–13.

9 M. Patel, R. Kumar, K. Kishor, T. Mlsna, C. U. Pittman and D. Mohan, Pharmaceuticals of emerging concern in aquatic systems : Chemistry, occurrence, effects, and removal methods, *Chem. Rev.*, 2019, **119**, 3510.

10 T. A. Der Beek, F.-A. Weber, A. Bergmann, S. Hickmann, I. Ebert, A. Hein and A. Küster, Pharmaceuticals in the environment — global occurrences and perspectives, *Environ. Toxicol. Chem.*, 2016, **35**, 823–835.

11 J. Lienert, T. Bürki and B. I. Escher, Reducing micropollutants with source control: substance flow analysis of 212 pharmaceuticals in faeces and urine, *Water Sci. Technol.*, 2007, **56**, 87–96.

12 EU Commision, European Union strategic approach to pharmaceuticals in the environment, *The Official Journal of the European Union (Eur-Lex)*, 2019, vol. 128, p. 13.

13 D. Awfa, M. Ateia, M. Fujii, M. S. Johnson and C. Yoshimura, Photodegradation of pharmaceuticals and personal care products in water treatment using carbonaceous-TiO2composites: A critical review of recent literature, *Water Res.*, 2018, **142**, 26–45.

14 A. A. Basheer, New generation nano-adsorbents for the removal of emerging contaminants in water, *J. Mol. Liq.*, 2018, **261**, 583–593.

15 D. Kanakaraju, B. D. Glass and M. Oelgemöller, Advanced oxidation process-mediated removal of pharmaceuticals from water: A review, *J. Environ. Manage.*, 2018, **219**, 189–207.

16 J. R. De Andrade, M. F. Oliveira, M. G. C. Da Silva and M. G. A. Vieira, Adsorption of pharmaceuticals from water and wastewater using nonconventional low-cost materials: A review, *Ind. Eng. Chem. Res.*, 2018, **57**, 3103–3127.

17 S. Das, N. M. Ray, J. Wan, A. Khan, T. Chakraborty, A. Khan and M. B. Ray, Micropollutants in wastewater: Fate and removal processes, in *Physico-Chemical Wastewater Treatment and Resource Recovery*, ed. R. Farooq and Z. Ahmad, IntechOpen, Croatia, 2017, pp. 75–107.

18 K. A. Thompson, K. K. Shimabuku, J. P. Kearns, D. R. U. Knappe, R. S. Summers and S. M. Cook, Environmental comparison of biochar and activated carbon for tertiary wastewater treatment, *Environ. Sci. Technol.*, 2016, **50**, 11253–11262.

19 N. Puri, A. Gupta and A. Mishra, Recent advances on nano-adsorbents and nanomembranes for the remediation of water, *J. Cleaner Prod.*, 2021, **322**, 129051.

20 M. N. Faiz Norrrahim, N. A. Mohd Kasim, V. F. Knight, M. S. Mohamad Misenan, N. Janudin, N. A. Ahmad Shah, N. Kasim, W. Y. Wan Yusoff, S. A. Mohd Noor, S. H. Jamal, K. K. Ong and W. M. Z. W. Yunus, Nanocellulose: a bioadsorbent for chemical contaminant remediation, *RSC Adv.*, 2021, **11**, 7347–7368.

21 R. E. Abouzeid, R. Khiari, N. El-Wakil and A. Dufresne, Current state and new trends in the use of cellulose nanomaterials for wastewater treatment, *Biomacromolecules*, 2019, **20**, 573–597.

22 S. Hokkanen, A. Bhatnagar and M. Sillanpää, A review on modification methods to cellulose-based adsorbents to improve adsorption capacity, *Water Res.*, 2016, **91**, 156–173.

23 N. Mohammed, N. Grishkewich and K. C. Tam, Cellulose nanomaterials: Promising sustainable nanomaterials for application in water/wastewater treatment processes, *Environ. Sci.: Nano*, 2018, **5**, 623–658.

24 A. Qiao, M. Cui, R. Huang, G. Ding, W. Qi, Z. He, J. J. Klemeš and R. Su, Advances in nanocellulose-based materials as adsorbents of heavy metals and dyes, *Carbohydr. Polym.*, 2021, **272**, 118471.

25 Y. Liu, C. Jin, Z. Yang, G. Wu, G. Liu and Z. Kong, Recent advances in lignin-based porous materials for pollutants removal from wastewater, *Int. J. Biol. Macromol.*, 2021, **187**, 880–891.

26 N. Supanchaiyamat, K. Jetsrisuparb, J. T. N. Knijnenburg, D. C. W. Tsang and A. J. Hunt, Lignin materials for adsorption: Current trend, perspectives and opportunities, *Bioresour. Technol.*, 2019, **272**, 570–581.

27 UNESCO and HELCOM, *Pharmaceuticals in the aquatic environment of the Baltic Sea region: A Status Report*, *Pharmaceuticals in the aquatic environment of the Baltic Sea region: A Status Report*, UNESCO Publishing, Paris, 2017.

2018 | *Environ. Sci.: Nano*, 2022, **9**, 2006–2019

This journal is © The Royal Society of Chemistry 2022

28 P. Figueiredo, M. H. Lahtinen, M. B. Agustin, M. De Carvalho, S. Hirvonen, P. A. Penttilä and K. S. Mikkonen, Green fabrication approaches of lignin nanoparticles from different technical lignins : A comparison study, *ChemSusChem*, 2021, **14**, 1–14.

29 A. Skogberg, A. J. Mäki, M. Mettänen, P. Lahtinen and P. Kallio, Cellulose nanofiber alignment using evaporation-induced droplet-casting, and cell alignment on aligned nanocellulose surfaces, *Biomacromolecules*, 2017, **18**, 3936–3953.

30 P. Lahtinen, S. Liukkonen, J. Pere, A. Sneck and H. Kangas, A Comparative study of fibrillated fibers from different mechanical and chemical pulps, *BioResources*, 2014, **9**, 2115–2127.

31 M. Farooq, T. Zou, G. Riviere, M. H. Sipponen and M. Österberg, Strong, ductile, and waterproof cellulose nanofibril composite films with colloidal lignin particles, *Biomacromolecules*, 2019, **20**, 693–704.

32 F. Kong, K. Parhiala, S. Wang and P. Fatehi, Preparation of cationic softwood kraft lignin and its application in dye removal, *Eur. Polym. J.*, 2015, **67**, 335–345.

33 R. Wahlström, A. Kalliola, J. Heikkinen, H. Kyllönen and T. Tamminen, Lignin cationization with glycidyltrimethyl-ammonium chloride aiming at water purification applications, *Ind. Crops Prod.*, 2017, **104**, 188–194.

34 M. H. Sipponen, M. Smyth, T. Leskinen, L. S. Johansson and M. Österberg, All-lignin approach to prepare cationic colloidal lignin particles: Stabilization of durable Pickering emulsions, *Green Chem.*, 2017, **19**, 5831–5840.

35 T. Gillgren, M. Hedenström and L. J. Jönsson, Comparison of laccase-catalyzed cross-linking of organosolv lignin and lignosulfonates, *Int. J. Biol. Macromol.*, 2017, **105**, 438–446.

36 P. S. B. do Santos, X. Erdocia, D. A. Gatto and J. Labidi, Characterisation of Kraft lignin separated by gradient acid precipitation, *Ind. Crops Prod.*, 2014, **55**, 149–154.

37 C. M. Maguire, Characterisation of particles in solution – a perspective on light scattering and comparative technologies, *Sci. Technol. Adv. Mater.*, 2018, **19**, 732–745.

38 L. Matsakas, M. Gerber, L. Yu, U. Rova and P. Christakopoulos, Preparation of low carbon impact lignin nanoparticles with controllable size by using different strategies for particles recovery, *Ind. Crops Prod.*, 2020, **147**, 112243.

39 M. Weiss, J. Fan, M. Claudel, T. Sonntag, P. Didier, C. Ronzani and L. Lebeau, Density of surface charge is a more predictive factor of the toxicity of cationic carbon nanoparticles than zeta potential, *J. Nanobiotechnol.*, 2021, **19**, 1–18.

40 I. Solala, M. C. Iglesias and M. S. Peresin, On the potential of lignin-containing cellulose nanofibrils (LCNFs): a review on properties and applications, *Cellulose*, 2020, **27**, 1853–1877.

41 T. Saito, S. Kimura, Y. Nishiyama and A. Isogai, Cellulose nanofibers prepared by TEMPO-mediated oxidation of native cellulose, *Biomacromolecules*, 2007, **8**, 2485–2491.

42 M. E. A. El-sayed, Nanoadsorbents for water and wastewater remediation, *Sci. Total Environ.*, 2020, **739**, 139903.

43 L. Zhao, J. Deng, P. Sun, J. Liu, Y. Ji, N. Nakada, Z. Qiao, H. Tanaka and Y. Yang, Nanomaterials for treating emerging contaminants in water by adsorption and photocatalysis: Systematic review and bibliometric analysis, *Sci. Total Environ.*, 2018, **627**, 1253–1263.

44 M. Thommes, K. Kaneko, A. V. Neimark, J. P. Olivier, F. Rodriguez-Reinoso, J. Rouquerol and K. S. W. Sing, Physisorption of gases, with special reference to the evaluation of surface area and pore size distribution (IUPAC Technical Report), *Pure Appl. Chem.*, 2015, **87**, 1051–1069.

45 S. Brunauer, L. S. Deming, D. W. Edward and E. Teller, On a theory of the van der Waals Adsorption of Gases, *J. Am. Chem. Soc.*, 1940, **62**, 1723–1732.

46 V. Kårelid, G. Larsson and B. Björlenius, Pilot-scale removal of pharmaceuticals in municipal wastewater: Comparison of granular and powdered activated carbon treatment at three wastewater treatment plants, *J. Environ. Manage.*, 2017, **193**, 491–502.

This journal is © The Royal Society of Chemistry 2022

Environ. Sci.: Nano, 2022, **9**, 2006–2019 | **2019**